Using hydroacoustic stations as water column seismometers

Selda Yildiz,[1] Karim Sabra,[2] LeRoy M. Dorman,[1,3] and W. A. Kuperman[1]

Received 1 February 2013; revised 15 March 2013; accepted 15 March 2013; published 7 June 2013.

[1] Getting seismic data from the deep oceans usually involves ocean-bottom seismometers, but hydrophone arrays may provide a practical alternative means of obtaining vector data. We here explore this possibility using hydrophone stations of the International Monitoring System, which have been used to study icebergs and T-wave propagation among others. These stations consist of three hydrophones at about the depth of the deep sound channel in a horizontal triangle array with 2 km sides. We use data from these stations in the very low-frequency regime (0.01–0.05 Hz band) to demonstrate that these stations can also be used as water column seismometers. By differencing the acoustic pressure, we obtain vector quantities analogous to what a seismometer would record. Comparing processed hydrophone station records of the 2004 Great Sumatra-Andaman Earthquake with broadband seismograms from a nearby island station, we find that the differenced hydrophones are indeed a practical surrogate for seismometers. **Citation:** Yildiz, S., K. Sabra, L. M. Dorman, and W. A. Kuperman (2013), Using hydroacoustic stations as water column seismometers, *Geophys. Res. Lett.*, *40*, 2573–2578, doi:10.1002/grl.50371.

1. Introduction

[2] Earthquake seismology suffers from an extreme continental bias. While broadband seismometers on islands fill some of the holes in coverage, vast tracts of the deep ocean remain uninstrumented. Getting seismic data from the deep ocean typically requires ocean-bottom seismometers, with all the deployment, coupling, and data recovery problems inherent in such instruments. Hydrophones, on the contrary, are intrinsically simpler but provide only the scalar pressure rather than the vector quantity desired. However, it should be possible to simulate seismic data by taking the appropriate spatial derivative of data from tripartite hydrophone arrays in the ocean. Those derivatives could simply be approximated by taking first differences. Pressure sensors, therefore, spaced within a small fraction of a wavelength of each other can be used to measure particle displacement, velocity, or acceleration analogous to measurements from a seismometer.

[3] Recent trends in ocean acoustics include ocean remote sensing methodologies [e.g., *Matsumoto et al.*, 2011] with data sampling rates and navigation accuracy substantially higher than seismic requirements. The method demonstrated in this paper, therefore, provides a potential opportunity to employ this technology in deep water regions for supplemental seismic measurements and also giving more flexibility in station coverage.

[4] The International Monitoring System (IMS) is a valuable source for studying a broad range of scientific problems in the oceans: monitoring acoustics of nuclear explosions [*Lawrence and Grenard*, 1998], estimating the rupture length of the December 2004 Great Sumatra earthquake [*de Groot-Hedlin*, 2005], T-wave propagation [*Tolstoy and Bohnenstiehl*, 2006], shipping noise [*Tolstoy and Bohnenstiehl*, 2002], seismo-acoustics of ice sheets [*Chapp et al.*, 2005], and localization of Antarctic ice-breaking events [*Li and Gavrilov*, 2008]. These studies, however, are at frequencies above 1 Hz and are predominantly of T-waves, which are generated by earthquakes along the plate margins [*Graeber and Piserchia*, 2004].

[5] In this paper, we show how low-frequency vector seismic data can be extracted from hydrophone array data by computing pressure gradients. From the appropriate pressure gradient records, we can simulate vertical, radial, and transverse velocity traces, although the transverse traces will not show Love waves since Love waves do not couple significantly into the water column as the viscous slip layer in the water column is only on the order of 10 m [*Fehler*, 1982]. We test this concept by processing hydroacoustic data from Comprehensive Nuclear-Test-Ban Treaty Organization's (CTBTO) IMS stations in the Indian Ocean and comparing the obtained simulated seismograms to velocity records from a nearby island seismic station. We demonstrate the procedure with simple analyses of records of the Great Sumatra-Andaman Earthquake of 2004 and show that water column data can be used to emulate seismometer measurements.

2. Vector Sensor Emulation From the IMS Hydrophone Triad

[6] The IMS hydroacoustic stations are designed horizontally in triplets with sides of approximately 2 km length; each station is deployed at or near the depth of the deep sound channel. To be able to use the hydroacoustic stations at this low frequency regime (f = 0.01–0.05 Hz), hydrophone data are transformed to vector velocity using pressure gradients. Measuring the pressure gradient between two closely separated (with respect to wavelength) points is equivalent to a velocity measurement [*Jensen et al.*, 2011]. Referring to Figure 1, we take this velocity sensor to be located at the center of the three hydrophones and

[1]Marine Physical Laboratory, Scripps Institution of Oceanography, University of California, San Diego, La Jolla, California, USA.
[2]School of Mechanical Engineering, Georgia Institute of Technology, Atlanta, Georgia, USA.
[3]Geosciences Research Division, Scripps Institution of Oceanography, University of California, San Diego, La Jolla, California, USA.

Corresponding author: S. Yildiz, Marine Physical Laboratory, Scripps Institution of Oceanography, University of California, San Diego, La Jolla, California 92093-0238, USA. (syildiz@ucsd.edu)

0094-8276/13/10.1002/grl.50371

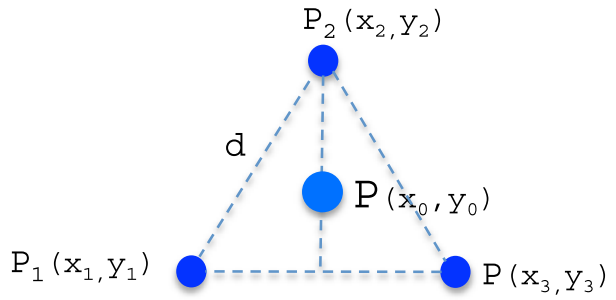

Figure 1. Pressure gradient representation for a hydroacoustic triad station with d =2 km sides. The three hydrophone configuration allows one to compute pressure and the three velocity components at the affective center of the hydroacoustic station at the very low frequency regime (f <0.1 Hz).

use a Taylor series expansion of the acoustic pressure field between each couple of hydrophones j and k as

$$P_j = P_k + \frac{\partial P}{\partial x}(x_j - x_k) + \frac{\partial P}{\partial y}(y_j - y_k). \quad (1)$$

Solution of pressure gradient in x and y includes a set of six equations where $j = 1, 2, 3$, $k = 1, 2, 3$, and $j \neq k$. The particle velocity components v_x and v_y can be obtained using the relationship between the gradient of acoustic pressure and the particle velocity as

$$v = -\frac{i}{\omega\rho}\nabla P, \quad (2)$$

where ω is the angular frequency and ρ is the local ambient density of the fluid medium. The vertical particle velocity component v_z is measured using depth differences of hydrophones in each station. To get the radial and transverse components of the velocity relative to a specified direction, v_x and v_y are rotated based on azimuthal angle.

3. Hydroacoustic Versus Seismic Data

3.1. Great Sumatra Earthquake

[7] In this section, we compare the IMS hydroacoustic data from the 26 December 2004, Mw=9.1 Sumatra earthquake with seismograph data of the same event, available from Global Seismic Network (GSN) of the Incorporated Research Institutions for Seismology (IRIS). Given the large magnitude of this earthquake, clear arrivals were recorded by the hydroacoustic stations at very low frequencies even though the hydroacoustic station data processing is not typically intended for these

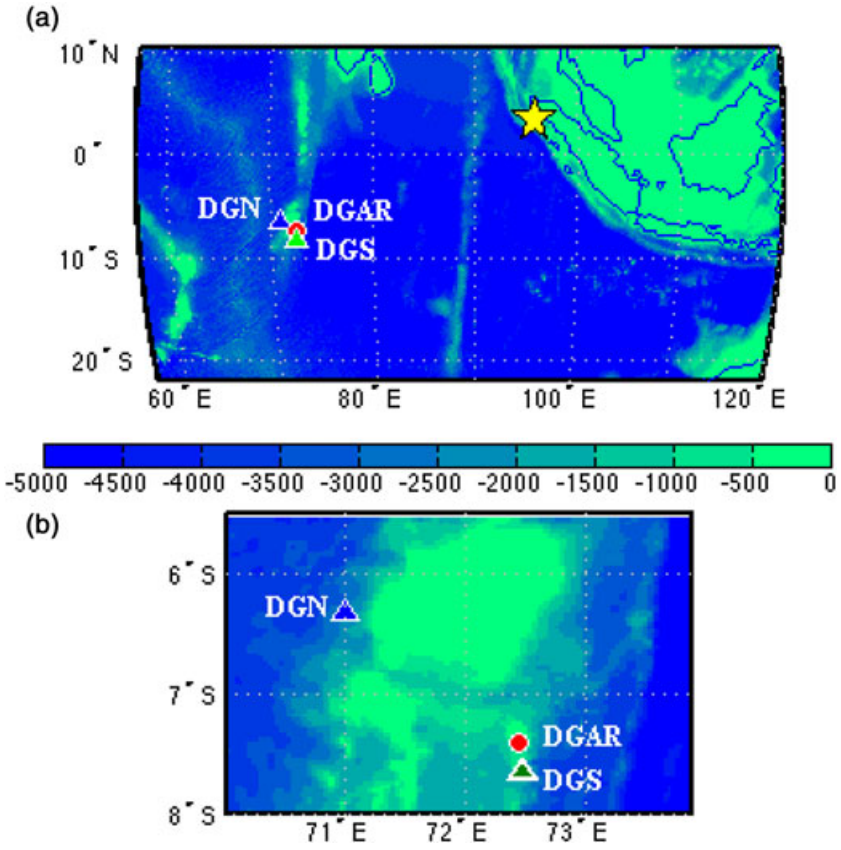

Figure 2. Maps of the study region using Smith and Sandwell bathymetry. Color bar indicates seafloor depth in meters relative to sea level, with 500 m contour intervals. (a) Main shock of the Sumatra earthquake is symbolized with yellow star. Blue triangle indicates Diego Garcia North hydrophone triad, DGN (6.30°S, 71.00°E); green triangle indicates Diego Garcia South hydrophone triad, DGS (7.60S, 72.50E). Red circle labeled as DGAR (7.41°S, 72.45°E) is the seismic station on the Diego Garcia Island. The DGN, DGS, and DGAR are located ~2970 km, ~2870 km, and ~2865 km to the southwest of the earthquake location, respectively. (b) Map of the Diego Garcia region in details. The DGN and DGS are located ~200 km to the northwest and ~25 km to the south of the DGAR, respectively.

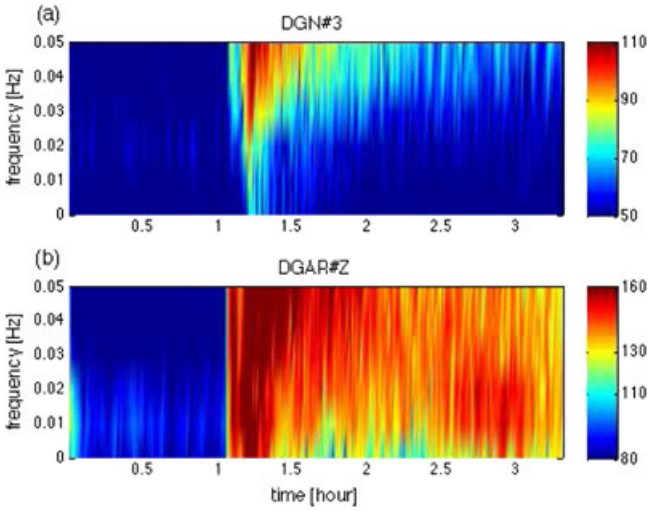

Figure 3. Spectrogram of (a) the pressure recorded on the third hydrophone DGN (i = 3) only (b) the vertical component of DGAR seismic station.

low frequencies. However, we have corrected the frequency response of the instruments, using the filter characteristics provided by CTBTO down to 0.1 Hz to be able to compare to the seismic station DGAR, so the results given here are recovered. Indeed, *Hanson and Bowman* [2005] have already used these single hydrophone IMS data to produce an unclipped spectrogram of the combined earthquake and subsequent tsunami arrival. We converted hydroacoustic and seismic data to Seismic Analysis Code (SAC) format and analyzed in SAC software [*Goldstein et al.*, 2003]. Arrival times are calculated using the TauP toolkit, Flexible Seismic Travel-Time, and Raypath Utilities [*Crotwell et al.*, 1999]. Given earthquake information (event location, time, and magnitude) and stations' location information, the TauP Toolkit embedded in SAC calculates arrival times of the body waves based on the earth-model embedded in the SAC toolbox.

[8] The study region is shown in Figure 2. The region ~70 km northwest of Diego Garcia is the Chagos Bank, the largest atoll structure in the world. The archipelago is a large bathymetric obstruction between northern stations, so signals observed at one triad might completely or partially be blocked at the other triad [*Hanson*, 2001]. We have used data from these stations in the very low frequency regime over 0.01–0.05 Hz band where the wavelengths of interest are above ~30 km. The depths of hydrophones at DGN station are 1248 m, 1243 m, and 1182 m, and at DGS station are 1413 m, 1356 m, and 1359 m, respectively. To determine the vertical component of particle velocity, v_z, we have used two particular hydrophones that give the maximum depth difference at each station. The depth difference of the hydrophones are taken as 66 m at DGN station and 57 m at DGS station.

[9] Figure 3 shows dynamic ranges of about 60 dB and 80 dB for the IMS station and adjacent seismometer station, respectively. This 20 dB difference in SNR indicates that the smallest earthquake detected by IMS station would be about one magnitude larger than for the seismic station.

3.2. Vector Sensor

[10] Applying equation (1) to hydroacoustic pressure data of f =0.01–0.05 Hz at DGN and DGS, we solve for three

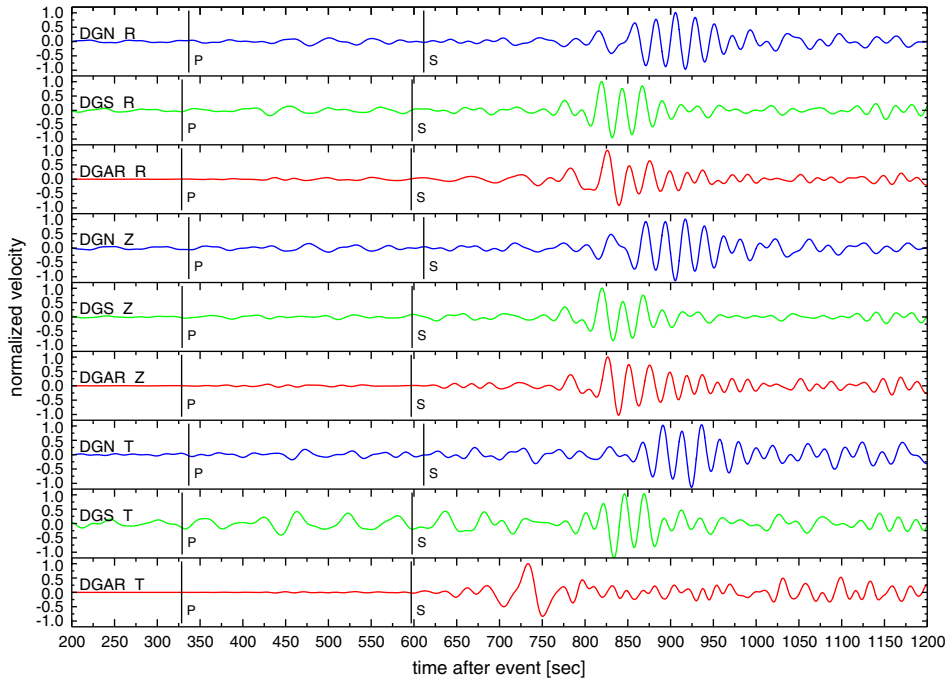

Figure 4. Hydroacoustic and seismic data of f =0.01–0.05 Hz are plotted using Seismic Analysis Code (SAC). R: Radial, Z: Vertical, T: Transverse. (top) Blue lines represent the DGN hydroacoustic data, (middle) green lines represent the DGS hydroacoustic data, and (bottom) red lines represent the DGAR seismic data. The x-axis corresponds to the time after event [200–1200 s], y-axis corresponds to normalized velocity. Arrival times of P and S waves calculated using TauP are indicated as black vertical lines on each time series.

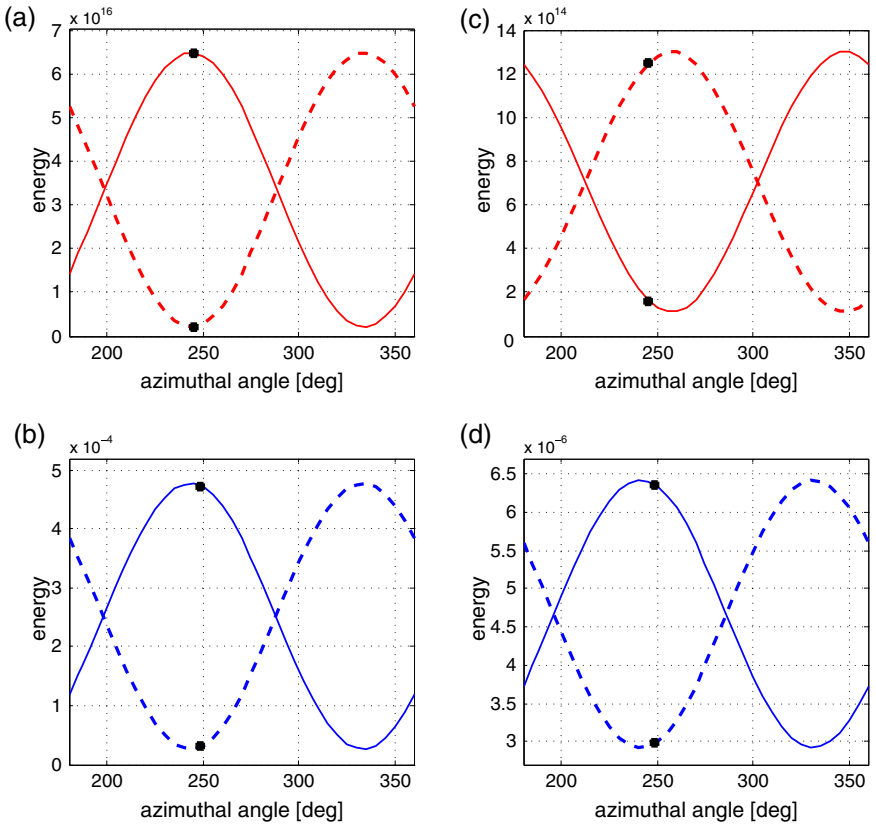

Figure 5. Optimized radial and transverse rotation results from (top) DGAR (red lines) and (bottom) DGN (blue lines). Continuous lines represent optimized radial, and dashed lines represent optimized transverse components. Black dots show the energy of the components at the true azimuthal angle. Radial rotation gives a maximum in radial component and a minimum in transverse component at both (a) DGAR and (b) DGN. Transverse rotation results (c) are reversed at DGAR and (d) do not show a significant change at DGN.

velocity components of the velocity v_x, v_y, and v_z. The three velocity components are normalized to the maximum of each to compare to the seismic data of the same frequency band. Figure 4 shows radial, vertical, and transverse velocities at both sites. Arrival times of *P* and *S* waves, calculated using the TauP toolkit, are indicated as black vertical lines on each time series.

[11] Referring to Figure 4, Rayleigh waves are dominant in the radial and vertical components at t = 800–1000 s for DGN, t = 750–950 s for DGS, and t = 750–950 s for DGAR seismic station, and match each other very well. Moreover, one can see the same arrival cycles at t = 750–850 s at both DGS and DGAR vertical components. Transverse components do not show a good agreement, which is consistent with the physics [*Fehler*, 1982], that the water column only supports longitudinal waves, and transverse Love waves do not couple into the water column. The comparison is also consistent with the relative locations noting that DGS is much closer to DGAR than DGN is.

[12] We have also generated synthetic mode seismograms to aid in the identification of seismic modes. The fundamental Rayleigh mode is large, as expected, arriving at DGAR at about 775 s (Figure 4). The synthetic seismogram for the one-dimensional preliminary reference earth model using the Mineos programs [*Masters et al.*, 2011] produces a fundamental mode of about 150 s in length. Adding nine overtones yields a packet of about 75 s in length, preceding the arrival of the fundamental mode. The data (Figure 4) show a similar behavior: the Rayleigh arrival is preceded by higher Rayleigh modes which are evident in the vertical components of DGS and DGAR. The match between DGS and DGAR at the onset of the Rayleigh arrival is consistent with them being located within a wavelength of each other.

[13] Looking at the DGAR transverse data (DGAR T) in Figure 4, the apparent transverse wave is significantly dominant at t = 700–750 s, whereas the radial wave (DGAR R) is small in the same time window. We have performed a rotation analysis, an example of which is shown in Figure 5, where north-south (x) and east-west (y) components of both hydroacoustic and seismic data are first rotated over the azimuth angles [180°–360°] to determine the direction of maximum response that should be equivalent to the radial and transverse directions. Here components rotated in each direction are called optimized radial, and components that are perpendicular to those are called optimized transverse. Then, the energy of optimized radial and transverse components at each direction are calculated at a specific time window and compared to the energy of the data at the true source direction. In Figure 5, we show the results from one of the hydroacoustic stations, DGN, and the seismic station, DGAR. For optimized radial plots, the rotation analysis time window is 800–1000 s for DGN, 750–950 s for DGAR, where the Rayleigh waves are dominant. As expected, rotating north-south and east-west velocity vectors gives a

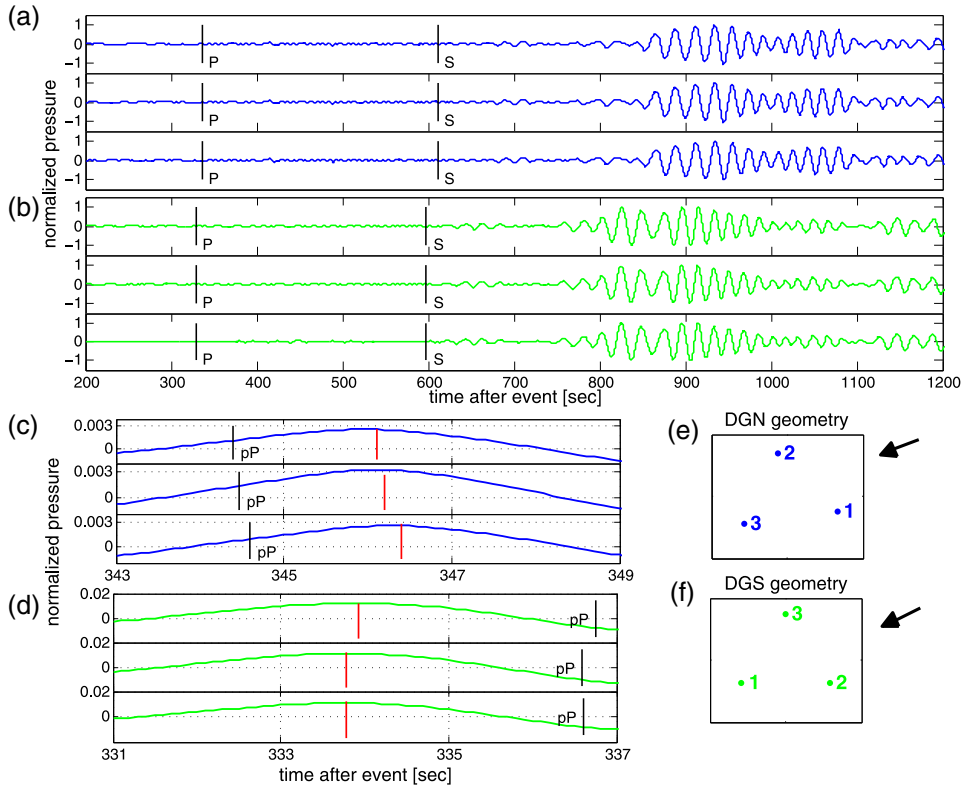

Figure 6. (a) DGN (blue lines) and (b) DGS (green lines) pressure data of f =0.01–0.05 Hz for hydrophones 1, 2, and 3, respectively. The x-axis corresponds to the time after event [200–1200 s], y-axis corresponds to the normalized pressure. (c) DGN pP-wave arrivals at 343–349 s and (d) DGS pP-wave arrivals at 331–337 s. Black and red vertical lines represent the predicted and observed arrival times of pP waves, respectively. Orientation of hydrophones and source signal direction (e) at DGN and (f) at DGS.

maximum in optimized radial components, and minimum in optimized transverse components in both hydroacoustic and seismic station Figures 5a and 5b. For optimized transverse plots, the time window was 710–780 s for DGN and 690–750 s for DGAR. When the transverse Love waves are dominant, as in DGAR seismic station, the rotation result is reversed, so a minimum in optimized radial components and a maximum in optimized transverse components is seen (Figure 5c). However, the same rotation process does not show significant change in the water column since we do not expect transverse coupling into the water column (Figure 5d).

[14] We have therefore demonstrated that hydroacoustic data at these low frequencies can be converted to seismic information. We can though also obtain the directional information from a slowness analysis of one IMS triad pressure data that is consistent with earthquake location.

3.3. Directionality from Slowness Analysis

[15] Previous work on slowness analysis of hydroacoustic data has been done in a higher frequency regime [*Graeber and Piserchia*, 2004]. In this work, we perform a slowness analysis of hydroacoustic data over 0.01–0.05 Hz band at the P-wave regime using three pressure data at both DGN and DGS. The pressure data in Figure 6a and 6b indicate that the waveforms are the same in all three hydrophones, and the predicted arrival times match the data. To localize the earthquake source location, delay times between each hydrophone pairs within a station are obtained from pP arrivals, which are well-identified because of their large signal to noise ratios (Figure 6c and 6d). These time delays are used to determine horizontal slowness components (p_x, p_y) and estimate the azimuth to the source region using

$$t = \Delta p, \tag{3}$$

where Δ is the geometric distance and t is the time difference between hydrophone pairs. This method [*Cansi*, 1995] assumes that the wavefront is a plane wave in the far field, and if the signals recorded at three sensors within a station are from the same source, then the sum of time delays (t_{12}, t_{23}, and t_{31}) should be close to zero, the closure relation. The measured time delays for DGN are t_{12} = –0.1 s, t_{23} = –0.2 s, and t_{31} = 0.3 s, and for DGS are t_{12} = 0.2 s, t_{23} = 0 s, and t_{31} = –0.2 s, and are indeed consistent with this closure relation.

[16] We have compared azimuthal angle obtained by slowness analysis with those predicted by SAC. From slowness analysis, the direction of propagation at the DGN and DGS are found to be 0.9° and 2.4° off from the direction predicted by SAC, respectively. The orientations of DGN, DGS, and source signal directions are shown in Figures 6e and 6f.

4. Conclusion

[17] We analyzed records of the Sumatra Earthquake of 2004 from two IMS hydrophone stations and a nearby GSN island station in the very low frequency band

(0.01–0.05 Hz). The hydroacoustic data were successfully converted to vector velocities comparable to seismic data. A spectral analysis of hydroacoustic and seismic data indicated that the magnitude of the smallest earthquake detectable by the tested IMS stations would need to be about one order of magnitude larger than what a conventional seismic station could detect. Vector sensor emulation from IMS hydrophone triads have shown to give essentially the same results as seismic data in radial and vertical motions at an adjacent land seismic station. Consistent with the physics, transverse Love waves in the water column do not couple, whereas *P* waves and Rayleigh waves with radial and vertical motion do couple. A slowness analysis based on longitudinal propagation physics in the water column permits the determination of the direction of the source location at a single IMS triad.

[18] **Acknowledgments.** We thank Mark Prior for providing access to hydroacoustic data collected by the Comprehensive Test-Ban Treaty Organization's International Monitoring System (CTBTO-IMS) and Mario Zampolli for providing frequency response characteristics of hydroacoustic stations. Information on the procedure for distribution of IMS data and data bulletins to Member States can be found at: [http://www.ctbto.org/verification-regime/the-international-data-centre/distribution-of-data-and-data-bulletins-to-member-states/]. Seismic data were retrieved from the Global Seismograph Network (GSN) via Incorporated Research Institution for Seismology (IRIS). We also would like to thank the reviewers for their detailed comments that helped improve the original manuscript.

References

Cansi, Y. (1995), An automatic seismic event processing for detection and location: The P.M.C.C. method, *Geophys. Res. Lett.*, *22*, 1021–1024.

Chapp, E., D. R. Bohnenstiehl, and M. Tolstoy (2005), Sound-channel observations of ice-generated tremor in the Indian Ocean, *Geochem. Geophys. Geosyst.*, *6*, Q06003, doi:10.1029/2004GC000889.

Crotwell, H. P., T. J. Owens, and J. Ritsema (1999), The TauP toolkit: Flexible seismic travel-time and ray-path utilities, *Seismological Res. Lett.*, *70*, 154–160.

de Groot-Hedlin, C. D. (2005), Estimation of the rupture length and velocity of the Great Sumatra earthquake of Dec 26, 2004 using hydroacoustic signals, *Geophys. Res. Lett.*, *32*, L11303, doi:10.1029/2005GL022695.

Fehler, M. (1982), Interaction of seismic waves with a viscous liquid layer, *Bull. Seism. Soc. Am.*, *72*, 55–72.

Goldstein, P., D. Dodge, M. Firpo, and L. Minner (2003), SAC2000: Signal processing and analysis tools for seismologists and engineers , in *Invited Contribution to The IASPEI International Handbook of Earthquake and Engineering Seismology*, edited by W. H. K. Lee, H. Kanamori, P. C. Jennings, and C. Kisslinger, Academic Press, London.

Graeber, F. M., and P.-F. Piserchia (2004), Hydroacoustic contributions to understanding the December 26th 2004, Zones of T-wave excitation in the NE Indian ocean mapped using variations in backazimuth over time obtained from multi-channel correlation of IMS hydrophone triplet data, *Geophys J. Int.*, *158*, 239–256.

Hanson, J. A. (2001), Earthquake location applied to a mini-array: K-spectrum versus correlation method, *23rd Seismic Research Review*, Jackson Hole, WY, Department of Energy. LA-UR-01-4454 (2), 12–22.

Hanson, J. A., and J. R. Bowman (2005), Dispersive and reflected tsunami signals from the 2004 Indian Ocean tsunami observed on hydrophones and seismic stations, *Geophys. Res. Lett.*, *32*, L17606, doi: 10.1029/2005GL023783.

Jensen, F. B., W. A. Kuperman, M. B. Porter, and H. Schmidt (2011), "Signals in noise", in *Computational Ocean Acoustics*, edited by W. M. Hartmann et al., pp. 750–754, Springer, New York.

Lawrence, M. W., and P. Grenard (1998), Hydroacoustic monitoring system for the Comprehensive Nuclear-Test-Ban Treaty, *OCEANS '98 Conference Proceedings*, *2*, 694–697, doi:10.1109/OCEANS.1998.724327.

Li, B., and A. Gavrilov (2008), Localization of Antarctic ice breaking events by frequency dispersion of the signals received at a single hydroacoustic station in the Indian Ocean, *J. Acoustic. Soc. Am*, *123*, 2990–2990.

Masters, G., M. Barmine, and S. Kientz (2011), Mineos version 1.0.2 user manual,CIG/CIT, 97, Pasadena, California, USA.

Matsumoto, H., J. H. Haxel, R. P. Dziak, D. R. Bohnenstiehl, and R. W. Embley (2011), Mapping the sound field of an erupting submarine volcano using an acoustic glider, *J. Acoustic. Soc. Am*, *129*, EL94–EL99, doi:10.1121/1.3547720.

Tolstoy, M., and D. R. Bohnenstiehl (2002), Analysis of hydroacoustic signals in the Indian Ocean. 24th Seismic Research Review, Nuclear Explosion Monitoring: Innovation and Integration, Sept. 2002.

Tolstoy, M., and D. R. Bohnenstiehl (2006), Hydroacoustic contributions to understanding the December 26th 2004 great Sumatra–Andaman Earthquake, *Surv. Geophys.*, *27*, 633–646.